ACCEPTED MANUSCRIPT • OPEN ACCESS

Multi-machine validation of plasma initiation modelling and prospects for future devicesPredicting plasma initiation using only hardware design and control room input data

To cite this article before publication: Hyun-Tae Kim *et al* 2026 *Nucl. Fusion* in press https://doi.org/10.1088/1741-4326/ae3caa

MULTI-MACHINE VALIDATION OF PLASMA INITIATION MODELLING AND PROSPECTS FOR FUTURE DEVICES

Predicting plasma initiation using only hardware design and control room input data

[1]Hyun-Tae Kim, [2]Eugenio Schuster, [3]Fabien Jaulmes, [1]Geoffrey Cunningham, [4]Gloria Falchetto, [5]Hong-Sik Yun, [6]James Yang, [7]Jeongwon Lee, [1]Joelle Mailloux, [1]Oliver Bardsley, [8]Peter de Vries, [9]Runze Chen, [10]Takuma Wakatsuki, [4]Xavier Litaudon, [5]Yeongsun Lee, [5]Yong-Su Na, and ITPA-Integrated Operation Scenario group

[1]UKAEA (United Kingdom Atomic Energy Authority), Culham Campus, Abingdon, Oxfordshire, OX14 3DB, UK
[2]Department of Mechanical Engineering and Mechanics, Lehigh University, Bethlehem, PA, United States of America
[3]Institute of Plasma Physics of the CAS, Za Slovankou 1782/3, 182 00 Prague 8, Czech Republic
[4]IRFM, CEA F-13108, Sant-Paul-lez-Durance, France
[5]Department of Nuclear Engineering, Seoul National University, Seoul, Korea, Republic Of
[6]Princeton Plasma Physics Laboratory, Princeton University, Princeton, NJ, United States of America
[7]Korea Institute of Fusion Energy, Daejeon, Korea, Republic Of
[8]ITER Organization, Route de Vinon sur Verdon, 13067 St Paul Lez Durance, France
[9]Institute of Plasma Physics, Chinese Academy of Sciences, Hefei, China
[10]National Institutes for Quantum Science and Technology, Naka 311-0193, Japan

Abstract

This paper reports on the generic prediction capability of full electromagnetic plasma initiation modelling with DYON, which was carried out for the first time in fusion research by the joint modelling of the International Tokamak Physics Activity (ITPA) - Integrating Operation Scenario (IOS) group. The following devices were included in the experiment database: VEST (spherical torus, copper coils, Stainless steel wall, R/a=0.3m/0.2m, V_v=3.7m^3), MAST-U (spherical torus, copper coils, C wall, R/a=0.7m/0.5m, V_v=55m^3), EAST (conventional tokamak, superconducting coils, metallic wall, R/a=1.85m/0.5m, V_v=38m^3), DIII-D (conventional tokamak, copper coils, C wall, R/a=1.67m/0.65m, V_v=35m^3), and KSTAR (conventional tokamak, superconducting coils, C wall, R/a=1.8m/0.5m, V_v=55m^3). Despite the different hardware features of the devices, the required operating spaces of the loop voltage induction and prefill gas pressure for inductive plasma initiation in each device were successfully reproduced by the predictive simulations with DYON using only the individual hardware design and the control room input data for each discharge. This successful validation across multiple machines demonstrates that the full electromagnetic DYON modelling can capture the essential physics of inductive plasma initiation. The simulation settings commonly employed for all modelling and the modifications necessary to account for the discrepancies between individual devices are reported. Predictions for ITER based on the multi-machine validation indicate that a wide range of prefill gas pressures exists for the Townsend breakdown and the plasma burn-through (0.01 - 1.5mPa).

1. INTRODUCTION

To initiate a plasma in tokamaks, the prefilled fuel gas in the vacuum chamber should be ionised to a few % degree of ionisation (i.e. plasma breakdown), and the degree of ionisation should proceed to achieve 100% degree of ionisation, fully ionising not only the main fuel gas but also the low-Z impurities (i.e. plasma burn-through) [1].

The feasibility of plasma initiation is one of the most important aspects when designing a fusion device. The highest loop voltage throughout the plasma pulse is induced during the plasma initiation phase by fully charging and then rapidly decreasing the currents in the Central Solenoid (CS) and Poloidal Field (PF) coils. Therefore, the required specifications for the coils and power supplies depend on the feasibility of plasma initiation. In addition, the high loop voltage induces strong eddy currents, which may reduce loop voltage induction in the vacuum centre and degrade the magnetic field null configuration. The toroidal electrical conductivity of the vessel and surrounding supporting structures must also be considered in plasma initiation assessments.

In large superconducting tokamaks, such as ITER [2], EU-DEMO [3], and STEP [4], the inductive plasma initiation will be challenging due to the large vacuum volume and the limited loop voltage [2]. To ensure the feasibility of plasma initiation during the design process and to optimise the operating scenario, it is important to develop and validate a reliable prediction tool that takes into account both the machine's hardware design and the control room input data i.e. coil currents and prefill gas pressure. Using the Electron Cyclotron (EC) wave for pre-ionisation and heating assistance facilitates the plasma initiation; however, EC modelling still requires further improvement and validation. In order to reduce the uncertainty in plasma initiation predictions involving integrated EC models, it is also important to confirm the validity of the inductive plasma initiation model alone.

The physics issues in the plasma burn-through phase were first reported in [5] and a mathematical model for 0D plasma burn-through simulations was published in [6]. Based on this, several physics models were further enhanced, and the DYON code has been developed, successfully reproducing the experimental data of a successful plasma burn-through discharge in JET [7]. DYON solves a system of differential equations representing the global energy and particle balances of electrons, the main fuel gas and impurities in each charge state. DYON calculates both the parallel and perpendicular transport of energy and particles with respect to the magnetic field lines, which evolve from a fully open configuration to Closed Flux Surfaces (CFSs) in the plasma initiation phase. The recycling of main fuels and the sputtering of wall impurities (carbon wall [7] and beryllium wall [8]) is calculated using the outward ion particle flux and a plasma-wall interaction model.

DYON and other mainstream plasma burn-through modelling codes in the fusion community (SCENPLINT [9] and BKD0 [10]) were compared by the joint code benchmark activity conducted by the International Tokamak Physics Activity - Integrated Operation Scenario (ITPA-IOS) group [11]. Before the code benchmark, the plasma burn-through modeling codes required the loop voltage waveform as input data and necessitated certain assumptions about the plasma volume. Additionally, a successful plasma breakdown was a necessary initial condition. In the code benchmark activity, the importance of the full electromagnetic modelling was identified, and the full circuit equations describing all toroidally conducting vessel structures, CS, and PF coils have been integrated into DYON [12]. This full electromagnetic feature enables the modelling of the vessel eddy currents and the calculation of the loop voltage in the plasma region with the CS and PF currents. Implementation of the full circuit equations enables the time evolution of the 2D poloidal magnetic flux map (i.e. ψ map) to be simulated in the vacuum space, with and without plasmas. This enables the Townsend breakdown to be evalulated along individual field lines and the plasma volume to be calculated in the burn-through phase.

The inductive plasma initiation prediction capability of the full electromagnetic DYON has been validated individually in MAST-U [13], VEST [14], EAST [15], DIII-D, and KSTAR. To confirm the generic validity of DYON in predicting the operation space, the ITPA-IOS group conducted a multimachine validation using a consistent simulation setup. This paper reports on the multimachine validation results and on predictive simulations for the inductive plasma initiation in ITER, based on the validated simulation setup.

This paper is structured as follows: In Section 2, we present the operation spaces for plasma initiation, identified through parameter scan experiments conducted on the five devices. Section 3 describes the input data from the multimachine experiment database and the simulation setup. Section 4 displays the predictive simulation results for the five devices. Based on the simulation setup used to reproduce the operation spaces in these devices, predictive simulations for ITER were performed, with the results presented in Section 5. Finally, additional discussion and the conclusion are provided in Sections 6 and 7, respectively.

2. EXPERIMENT DATABASE

One of the key objectives of the multi-machine validation is to test whether the predictive model can capture the essential physics without adjusting any free parameters for each device, which has very different hardware features such as aspect ratio, coil types, first wall material, ferromagnetic material, vacuum volume, plasma volume, toroidal magnetic field, and the effective connection length. Table 1 lists the devices in the experiment databases, and summarises their features. Since the aspect ratio (conventional tokamak or spherical torus) and the coil types (copper coils or superconducting coils) are different, the control room signals (coil currents and gas pressure) are also all different in each device. As an example, Figure 1 compares the time traces of central solenoid current, gas pressure, loop voltage, and plasma current in the five devices. In order to validate the generic capability of predicting individual discharges and thus the operating space in such different devices, five dedicated experiment databases were established by scanning the prefill gas pressure p_0 and the induced loop voltage V_{loop}.

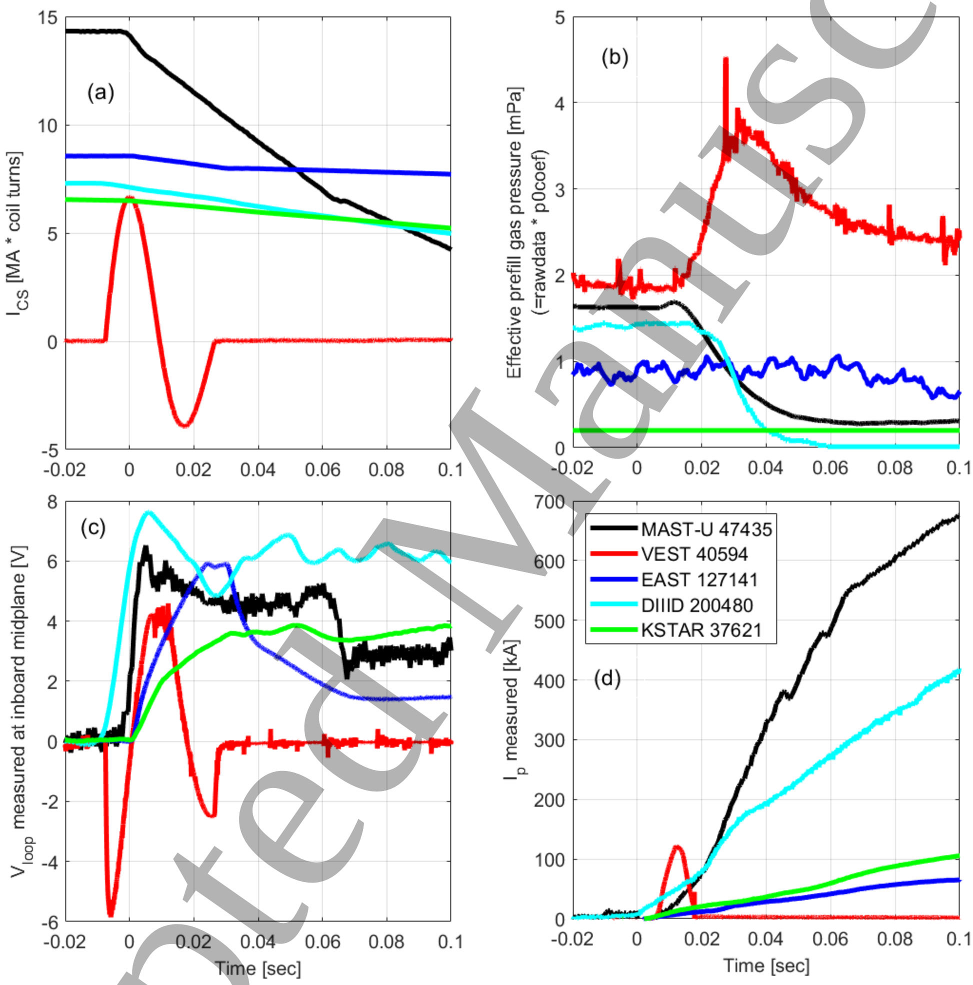

Figure 1(a) Central solenoid current × # of coil turns (b) fuel gas pressure (c) measured loop voltage, and (d) the measured plasma current in MAST-U, VEST, EAST, DIII-D, and KSTAR

Figure 2 shows the operation spaces for inductive plasma initiation identified in the experiment databases. In the experiments, the discharges that achieved a sufficient increase in I_p (a few tens of kA) following successful Townsend breakdown and plasma burn-through were defined as successful plasma initiation. If a strong D_a signal was detected without a sufficient increase in I_p, the discharge was defined as plasma burn-through failure. If there was no or a very weak D_a signal detected with virtually zero I_p, the discharge was defined as Townsend breakdown failure (i.e. failure in electron avalanche). In all devices, it was commonly observed that the lower p_0 limit of the operation space was determined by the Townsend breakdown failure, while the upper p_0 limit and the lower V_{loop} limit are determined by the plasma burn-through failure. In the fusion community, the operation space for Townsend breakdown is often conventionally estimated using the Paschen curve, which is calculated with the effective connection length $(L_f[\text{m}] = 0.25 \times a[m] \frac{B_\phi[T]}{B_\perp[T]})$ and the Townsend breakdown criteria$(V_{loop}[V] = 2\pi R[m] \times \frac{93.76 \times p_0[Pa]}{\ln(3.83 \times p_0[Pa] \times L_f[m])})$ [1]. The Paschen curves in Figure 2 were calculated with the parameters in Table 1 and the assumption of $B_\perp$= 1mT, which is to represent a good magnetic field null. 1mT is a reasonable average value, as one can also see that a similar value was calculated in DIII-D (1.5mT) [16] [17]. In all devices, the lower p_0 limits in Paschen curves are positioned far higher than the p_0 in the failed breakdown discharges in experiments. This suggests that L_f is not a valid measure to predict the operation space for Townsend breakdown, and a more complete calculation with modelling is necessary.

One might be able to improve the stray field assumption (i.e. $B_\perp = 1mT$) by taking a null region boundary circumference-weighted average in individual discharges, as proposed in [17]. However, the averaging calculation does not reduce the order of magnitude of the estimated $B_\perp$ and the Paschen curve is still far deviated from the experimental data. Furthermore, it should be noted that there is an uncertainty about where $B_\perp$ should be averaged. As mentioned in [17], the plasma breakdown could take place at an inner radial position, which is far from the middle of the field null configuration. These indicate that the conventional calculation, simply taking a single averaged value and using it for Townsend breakdown criteria formula, is not appropriate for correctly predicting the operation space. Also, as was shown in [13], even if a few field lines meet the Townsend breakdown criteria, if the number of successful open field lines is too small, the plasma initiation could fail. To properly address these, assessing all individual field lines for Townsend breakdown criteria is necessary by performing a proper numerical modelling.

Table 1 Experiment databases for the multimachine validation of the operation space prediction of inductive plasma initiation (ST: Spherical Torus, CT: Conventional Tokamak).

Device	Vacuum space geometry	Coils	First wall material	Ferromagnetic material	$V_v[m^3]$	$V_p[m^3]$	$B_t[T]$	$L_f[m]$
MAST-U	ST (R=0.7m, a=0.5m)	Copper	C	N/A	55	6	0.6	75
EAST	CT (R=1.85m, a=0.5m)	Super Conductor	W + Mo	N/A	38	7.5	2.5	311
DIII-D	CT (R=1.67m, a=0.65m)	Copper	C	N/A	35	16	1.8	292
KSTAR	CT (R=1.8m, a=0.5m)	Super Conductor	C	Incoloy 908 in the jacket of PF and TF coils	55	7.5	1.8	315
VEST	ST (R=0.3m, a=0.2m)	Copper	Stainless steel	N/A	3.7	0.6	0.23	12

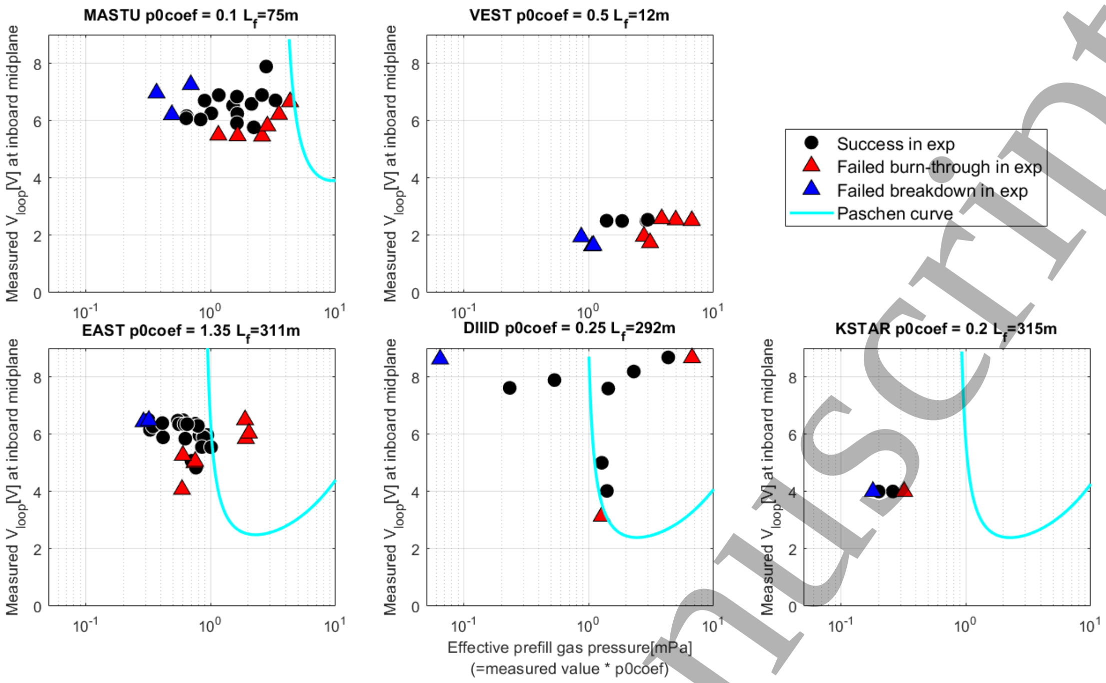

Figure 2 operation space for plasma initiation identified by scanning the loop voltage and the prefill gas pressure in MAST-U, VEST, EAST, DIII-D, and KSTAR experiments. Black circles: successful plasma initiation, Red triangles: plasma burn-through failure, and Blue triangles: Townsend breakdown failure, and cyan lines: Paschen curves (the Paschen curve in VEST is positioned far higher than the experimental data, so not shown in the figure).

3. INPUT DATA AND SIMULATION SETUP

3.1. Input data – machine description, coil currents, and prefill gas pressure

In order for systematic validation of the full electromagnetic DYON on multiple machines, the same modelling strategy was employed for all devices. First, the electromagnetic response of the conducting structures was calibrated to represent the 3D nature (e.g. ports in the vacuum vessel) in the 2D model. Figure 3 shows the active coils and the passive structures in the devices. By comparing the calculation of the induced loop voltage with the flux loop data, the resistivities of the passive structure elements were increased from the nominal values (e.g. 7.2e-7 [Ohm*meter] for Stainless steel), which is valid only if the passive structures are toroidally symmetric. Figure 4 shows the CS and PF coil currents used in the control room. Using the coil current input data and the calibrated machine description, the V_{loop} measured by the flux loop near the inboard mid-plane were successfully reproduced in the full electromagnetic DYON. This confirms the validity of the calibrated machine description.

The next step was to reproduce the plasma initiation phase in a reference discharge. The simulation results of plasma current, line radiation emission such as D_a, C-III, average T_e and n_e are then compared with the corresponding measured values. Examples of a reference discharge reproduction with DYON modelling are available in the previous publications (MAST-U [13] and EAST [15]). Based on the comparison with the experimental data, the prefill gas pressure value used in the modelling is corrected by multiplying it by a scaling factor (i.e. effective prefill gas pressure = p_0 coefficient x measured fast ion gauge data) to account for errors, possibly arising from the distance between the plasma and the pressure diagnostic system, or/and the calibration error of the fast ion gauge. Finding the p_0 coefficient requires a reference discharge in existing devices, but this is less of a problem for predicting future devices. The prefill gas pressure can be easily adjusted during operation. It is important to predict whether there is a feasible gas pressure range that is wide enough at the given hardware and coil current scenarios. The p_0 coefficients reproducing a reference discharge are given in Table 2.

Table 2 Simulation setup to take into account the features of each device

Device	Sputtering yield	Ferromagnetic modelling	p_0 coefficient
MASTU	0.1% initial O + C sputtering by D ions = 0.03	N/A	0.1
EAST	0.1% initial O	N/A	1.35
DIII-D	0.1% initial O + C sputtering by D ions = 0.03	N/A	0.25
KSTAR	0.1% initial O + C sputtering by D ions = 0.03	Done	0.2
VEST	0.1% initial O	N/A	0.5

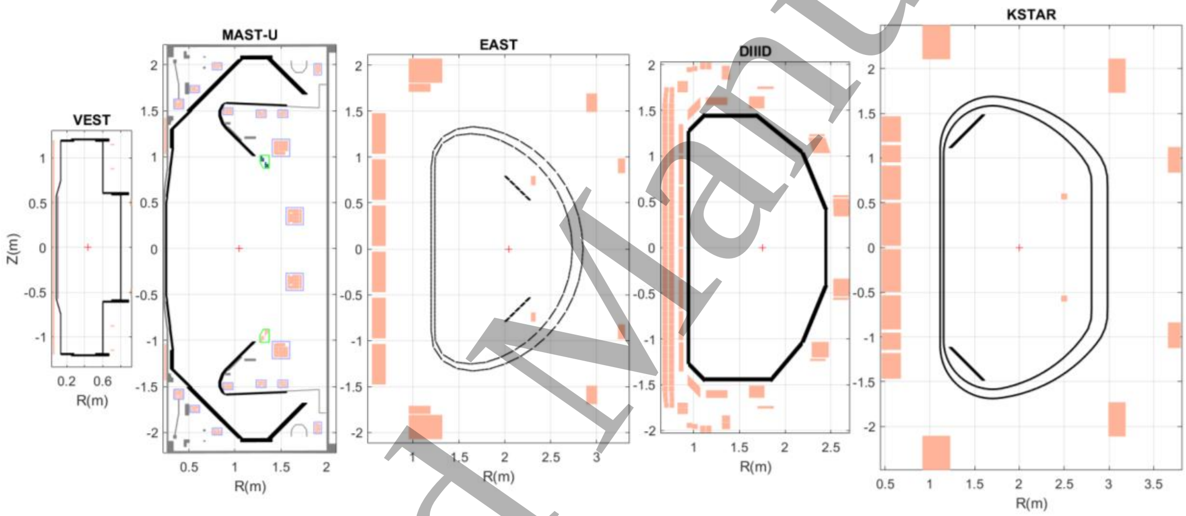

Figure 3 Description of CS and PF coils (in beige) and passive structures (in black, gray, or cyon) in the devices – VEST, MAST-U, EAST, DIII-D, and K-STAR

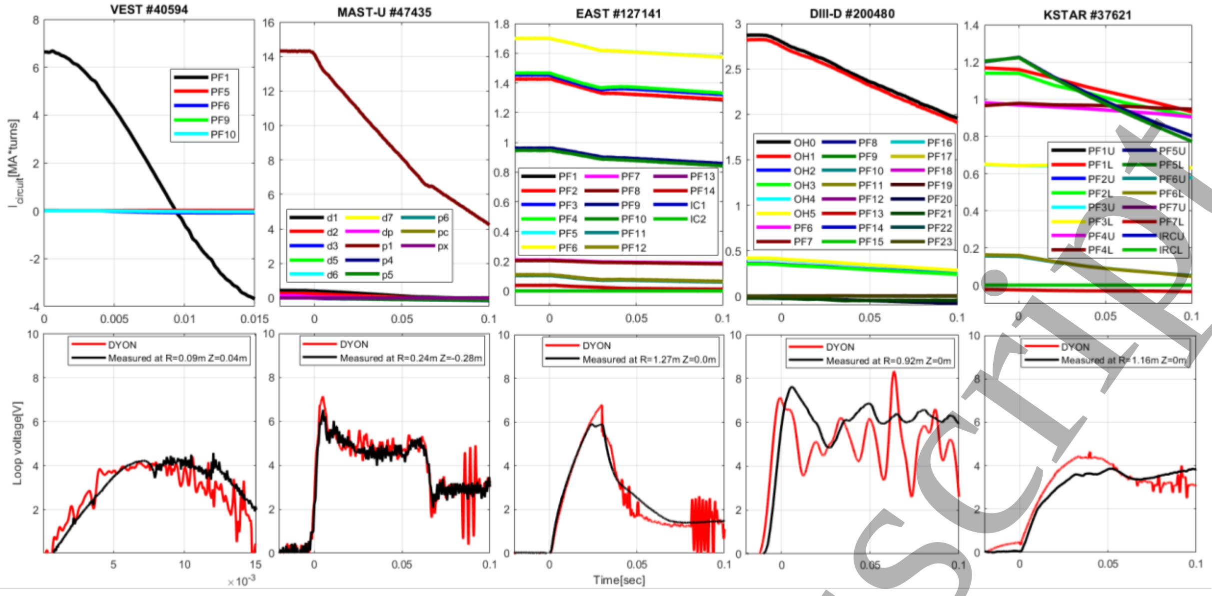

Figure 4 Coil currents and comparison of the loop voltages calculated (red) and the measured value (black) near the inboard mid-plane in each device – VEST, MAST-U, EAST, DIII-D, and K-STAR. (Note, the x-axis scale of VEST data is different to the other devices.)

3.2 Simulation setup

The choice of impurity sputtering models is subject to the first wall material in each device. The chemical sputtering from a metal first wall such as tungsten can be ignored, because the ion temperature in the burn-through phase is less than 100eV, whereas the threshold incident ion energy required for physical sputtering at the tungsten wall is much higher than 100eV. In the devices with a metal first wall, the main impurity source is the impurities remaining in the prefill gas or lightly attached to the wall from the previous discharges, which could be instantly released once the Townsend breakdown occurs. On the other hand, the carbon first wall is chemically active, and the chemical sputtering by D ions and low-Z impurity ions (e.g. oxygen) [7] should be modelled. The wall conditions of discharges in the experiment databases were managed using between-shot glow discharge cleaning or wall conditioning such as lithiumisation or boronisation. Therefore, it is reasonable to assume a low level of initial low-Z impurities in the prefill gas. Adjusting the initial low-Z impurity level in the modelling can help to better reproduce individual discharges. However, the initial impurity content is an uncertain parameter for future devices. To assess the generic prediction capability under the reasonable assumption of an initial low-Z impurity, the common initial oxygen of 0.1% in the prefill gas was used as the initial condition for modelling all devices.

Ferromagnetic material can distort the magnetic field configuration, degrading the null quality. KSTAR has a ferromagnetic material (Incoloy 908) in the jacket of the PF coils and all the Toroidal Field (TF) Coils [18]. To take into account the ferromagnetic effects, finite element method modelling of the nonlinear *B–H* curve of Incoloy 908 was performed, and the ferromagnetic 2D poloidal magnetic flux (i.e. ψ) was prescribed in the DYON modelling of KSTAR discharges. It was found that the prescribed ψ data were necessary for DYON to reproduce a successful plasma initiation in KSTAR #37621. *Figure 5* compares the magnetic field configuration calculated by DYON with and without the ferromagnetic 2D poloidal magnetic flux. Without the ferromagnetic correction, the magnetic field null is not formed in the vacuum centre, and the breakdown fails in DYON. Such a ferromagnetic correction will be necessary for plasma initiation modelling in future devices if they contain ferromagnetic materials such as Incoloy 908. However, ITER does not have Incoloy 908 so the ferromagnetic effects were not modelled in the DYON prediction of ITER in this paper.

Apart from those described in Table 2, all the discharges in the multi-machine database are simulated with the same simulation setup, without adjusting any free parameters for individual devices or discharges.

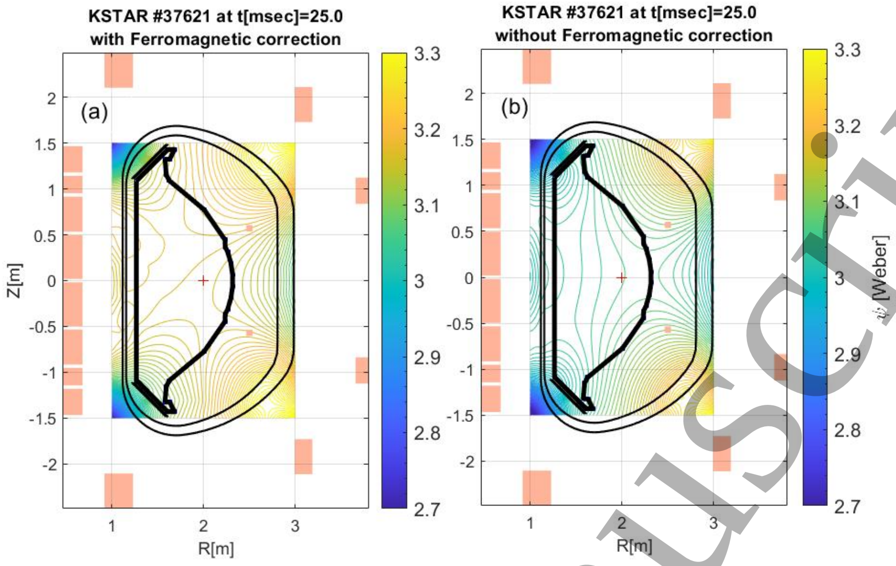

Figure 5 2D vacuum psi map of KSTAR #37621 calculated by DYON (a) with and (b) without the ferromagnetic correction

4. MULTIMACHINE VALIDATION RESULTS

The experiment databases reveal common features. The lower and the upper limits of p_0 are determined by the Townsend breakdown failure and the plasma burn-through failure, respectively. The lower limit of V_{loop} is determined by the plasma burn-through failure. Using only the control room input data of each discharge (i.e. currents in the CS, PF and TF coils, p_0, and the gas puffing rate) and with the simulation setup being the same for all devices apart from the parameters in Table 2, the full electromagnetic DYON correctly predicted the Townsend breakdown failure, plasma burn-through failure, and successful plasma initiation for most discharges in all devices (see Figure 6). This successful demonstration across multiple machines proves the generic capability of predicting the operating space for inductive plasma initiation.

A couple of the failed burn-through discharges in MAST-U and VEST experiments were predicted to be successful in the modelling. The incorrectly predicted discharges are closely positioned to the lower V_{loop} limit of the operation space. The incorrect prediction should be due to the 0.1% initial oxygen in the prefill gas, which was identically defined in all discharges to assess the generic prediction capability. When increasing the initial oxygen to 2%, the failed burn-through discharges in experiments were correctly predicted in the modelling.

The lower p_0 limit predicted by the modelling is generally close to that observed in experiments. However, predictions of individual failed breakdown discharges are often inaccurate, requiring slightly lower or higher p_0 values for correct prediction. This may be because the Townsend breakdown assessment of individual open field lines in the present modelling does not capture some additional breakdown physics, although it is much more accurate than the conventional estimation with L_f. For example, the space charge during the breakdown phase could produce strong self-generated electric fields that can increase the convection losses of electrons by ExB drift [19] and cancel the externally induced V_{loop} and reduce the collisional ionisation rate along the magnetic field lines [20]. Also, when assessing the Townsend breakdown, DYON used 0.5 x L_{open} (i.e. L_{open} is the calculated length of the individual open field lines). This factor 0.5 was adopted to estimate the actual travelling length of electrons, accounting for the arbitrary starting points of the seed electrons in open field lines. It has been reported that adjusting the factor helps to better reproduce the Townsend breakdown [21]. However, in order to take these additional physics into account in the modelling, some free parameters must be used for each device or discharge. For the purpose of the multimachine validation in this paper, the additional breakdown physics models were not adopted.

The impact of a higher initial oxygen content in the prefill gas was investigated by testing the operation space prediction in EAST (see Figure 7), which is the database with the environment closest to ITER among the multimachine databases, i.e. it has superconducting coils with a metal wall in a conventional tokamak geometry. Up to 1% initial oxygen content in the prefill gas, there is no significant change in the predicted operation space. However, as the oxygen content increases beyond 1%, the operation space shrinks gradually from the upper p_0 boundary. The assessment indicates that the EAST operation space is best reproduced in predictive modelling with a low initial oxygen content (0 - 1%), which can be justified by the lithiumisation of the first wall performed before the experiments. Lithium has a low threshold energy of incident ions for physical sputtering, so the impact of the physical sputtering of lithium was tested [15]. The predicted operation space was not changed at all by the lithium physical sputtering, because of the low radiation power of lithium ions. The ITER operation plan involves boronising the first wall to reduce the initial oxygen level [22]. In the modelling with the boron physical sputtering, the predicted operation space remains almost unchanged. However, it should be noted that the test modelling with physical sputtering of lithium or boron assumed no initial content of either element. While it has been reported that initial lithium in the prefill gas has little impact, a few % of initial boron could reduce the operation space [15].

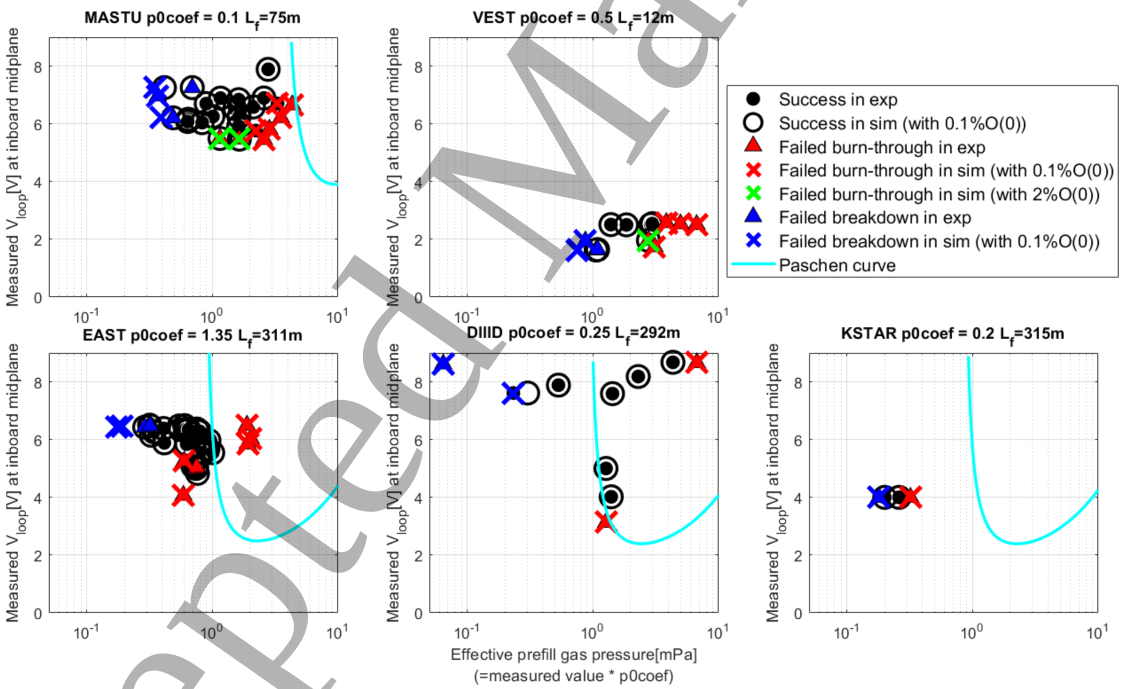

Figure 6 Operation space in the loop voltage at the inboard midplane and the effective prefill gas pressure for plasma initiation. The experimental data are indicated by filled black circles (successful plasma initiation), red triangles (plasma burn-through failure), and blue triangles (Townsend breakdown failure). The corresponding predictive simulation results are indicated by open black circles (successful plasma initiation), red crosses (plasma burn-through failure with the default simulation setup i.e. with 1% initial oxygen in the prefill gas, and blue crosses (Townsend breakdown

failure). The green crosses indicate the plasma burn-through failure in DYON with 2% initial oxygen. The cyon lines are Paschen curves calculated with $L_f\,(=0.25 * a\frac{Bt}{B\perp})$.

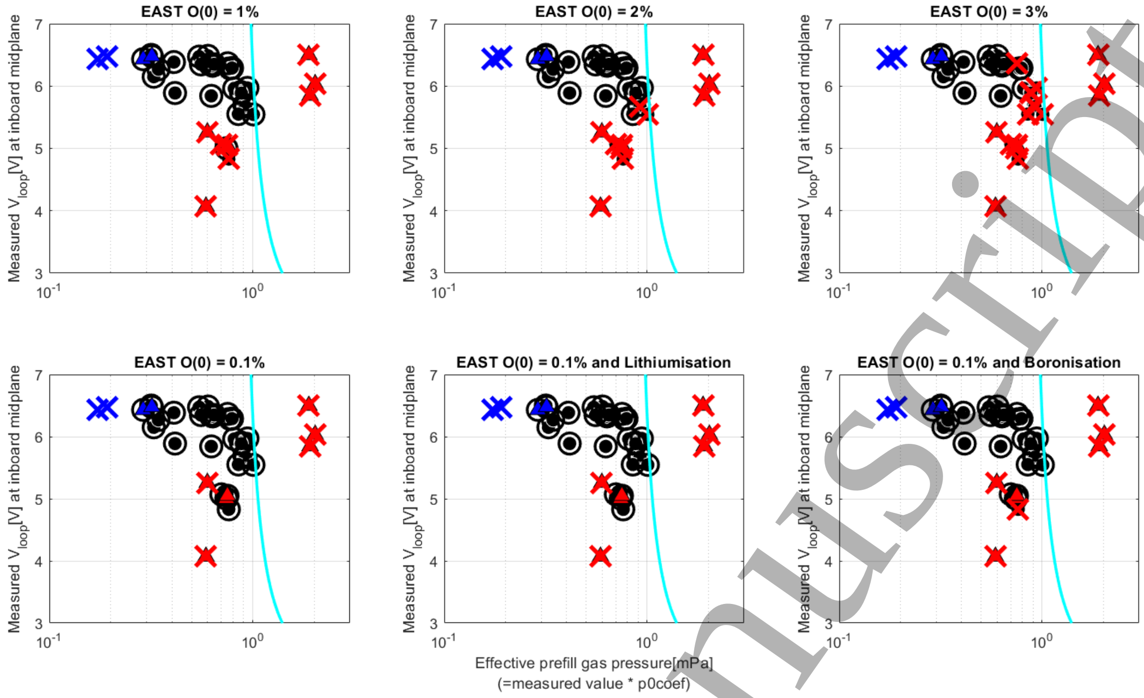

Figure 7 Operation spaces for plasma initiation with different initial oxygen and wall conditioning in EAST. The meaning of symbols is the same as Figure 6.

5. PREDICTION TO ITER

In the previous prediction, which did not take into account the full electromagnetic features, DYON predicted that the upper p_0 limit of plasma burn-through would be around 1mPa, and that the initial low-Z impurity content should be less than 1% for inductive plasma burn-through in ITER [23]. The same prediction results were obtained through modelling with SCENPLINT and BKD0 [11]. Predictive simulations of inductive plasma initiation in ITER have been performed again with the full electromagnetic DYON modelling. The machine description of ITER and the CS and PF currents (#105052) were obtained from the ITER Integrated Modelling and Analysis Suite (IMAS) [24]. Based on the EAST predictive modelling results, 0.1% initial oxygen and physical sputtering of boron were assumed. Figure 8 and Figure 9 (a)-(e) are the predictive simulation results at p_0=1mPa in ITER, and Figure 9(f) indicates the p_0 range for inductive plasma initiation. DYON predicted that the upper p_0 limit is 1.5mPa, which is slightly higher than the previous prediction.

In the present devices, the completion of plasma burn-through typically takes less than 20-30ms at most (e.g. < 20ms in MAST-U [13]). However, in ITER, which has a much larger vacuum volume, I_p can only begin to ramp up at 750ms, when the prefilled D gas has fully ionised. Until deuterium burn-through is completed, most of the electron energy from Ohmic heating is radiated, and T_e does not increase (i.e. the plasma resistance does not decrease). Due to the high plasma resistance at the low T_e, the induced loop voltage is resistively dissipated rather than increasing I_p, and only drives large eddy currents (~ 1.3MA). Oxygen 5+ becomes dominant at 950ms, indicating that the plasma burn-through phase would take around 1 second to complete in ITER.

Once the D burn-through phase is successfully completed, I_p begins to increase. CFSs are created when the poloidal field generated by I_p exceeds the perpendicular field from the external coils or eddy currents. In DYON, the ψ contributed by I_p is calculated using the filament current model, which is positioned in the middle of the vacuum space. Initially, the CFSs are only locally formed around the filament current, as I_p is still small. As the I_p increases, CFSs are formed globally. Conversely, as D neutrals are depleted during the burn-through phase, fewer open field lines meet the Townsend breakdown criteria. Therefore, during the transition from the burn-through phase to the I_p ramp-up phase, the plasma volume occupied by the open field lines is replaced by the volume occupied by CFSs, resulting in a dynamic evolution of the total plasma volume (see Figure 9(d)).

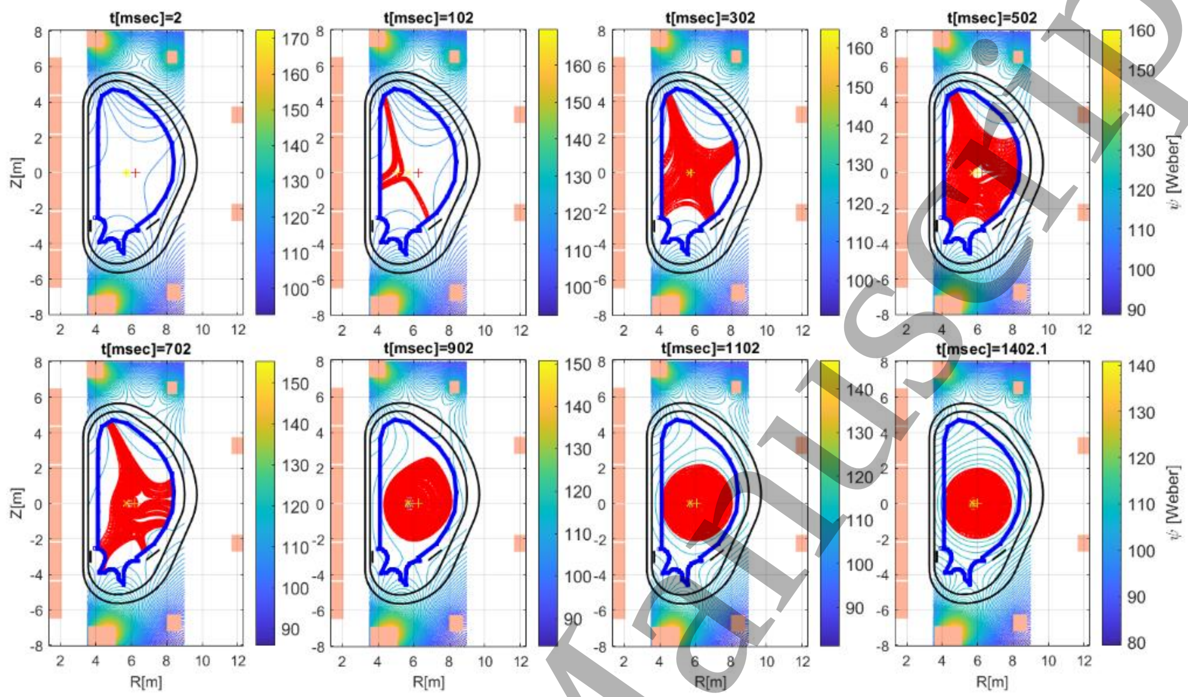

Figure 8 Example of psi map evolution of ITER plasma initiation, simulated with full electromagnetic DYON with the operation scenario of 105052, 1mPa, 0.1% initial oxygen, and boron physical sputtering

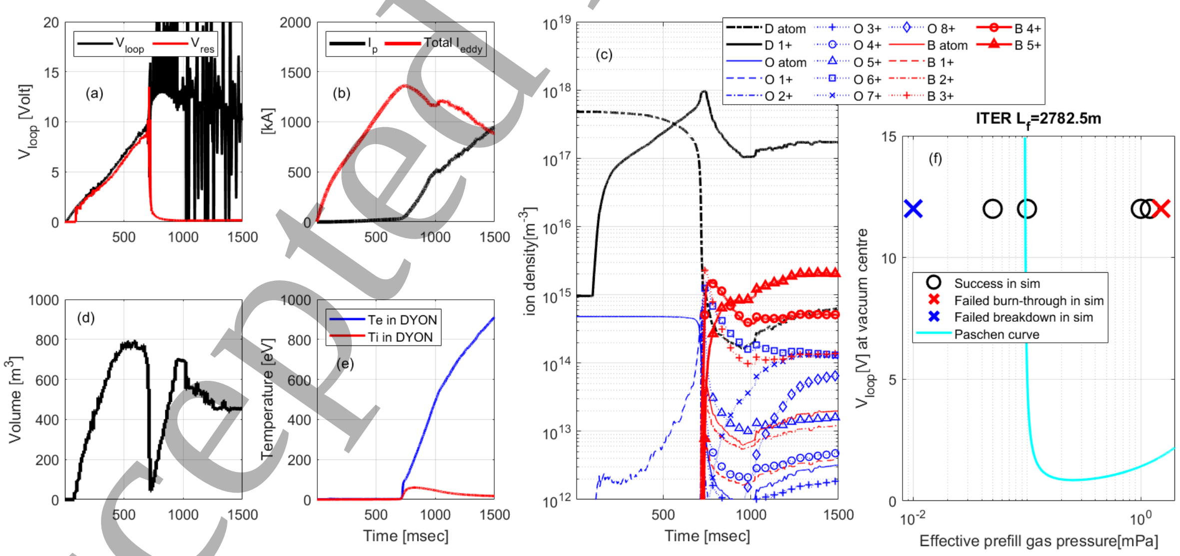

Figure 9 An example of DYON prediction of inductive plasma initiation in ITER (p_0=1mPa): (a)total induced loop voltage (black) and the resistive loop voltage(red), (b)plasma current (black) and total eddy current in the passive structures(red), (c)atom or ion densities of deuterium (black), oxygen(blue),

and boron(red), (d)plasma volume, (e)temperatures of electrons(blue) and ions(red), and (f) operation space for inductive plasma initiation in ITER

Figure 9(c) shows that the ionisation of the D neutrals begins at 100ms. The V_{loop} is induced from 0 seconds and only reaches 2 - 3V at around 100ms. This suggests that the Townsend breakdown criteria are easily met at V_{loop} much lower than the ITER hardware limit (i.e. 12 V). The lower p_0 limit estimated by the Paschen curve is 0.1mPa, which is approximately one order of magnitude lower than those in the current devices. This is because the connection length in ITER is about an order of magnitude longer than that in the existing devices. As observed in the multi-machine databases, the lower p_0 limit predicted by DYON modelling is also lower in ITER than the Paschen curve estimation.

Regarding the inductive operation space, the predictive modelling of plasma burn-through and Townsend breakdown indicates ITER has a wide range of p_0 for inductive plasma initiation (0.01mPa - 1.5mPa). However, it should be noted that we assumed effective boronisation of the first wall and a low level of initial impurity (0.1% initial oxygen in the prefill gas) in the ITER modelling. The initial oxygen level was scanned at 1mPa of p_0, and DYON predicts that plasma burn-through fails with 5% initial oxygen in ITER. In other words, the upper limits of p_0 should be lower than 1.5mPa if there are significant initial impurities.

Lastly, Figure 9(e) shows T_i does not increase during the I_p ramp-up phase. Such a decoupling of T_i from T_e is due to the low n_e during the I_p ramp-up phase. In the ITER simulation, no additional gas fuelling was defined, as the main purpose of the simulation is to predict the plasma breakdown and burn-through phases. In experiments, additional gas fuelling is provided once the burn-through phase is completed. The gas fuelling increases n_e, thereby increasing the equilibration power between T_e and T_i, and making T_i also increase. To extend the predictive modelling to the I_p ramp-up phase, the input data waveform of the effective gas puffing rate should be prescribed.

6. DISCUSSION

The DYON simulation without full electromagnetic modelling was first compared with JET data [7] [8]. However, JET data were not included in the experimental database for this paper, as the iron core in JET complicates the full electromagnetic simulation. To account for the impact of the iron core on the dynamic ψ map calculation, an additional model is required. Nevertheless, the current validation remains relevant for planned future devices (ITER, EU-DEMO, and STEP), as they do not include an iron core in the hardware design.

In the ITER simulation, DYON predicted a successful Townsend breakdown at a very low p_0 (0.01 – 0.1 mPa) due to the long connection length in ITER. Such a low p_0 facilitates the subsequent burn-through phase by reducing the required heating power to overcome the radiation barrier [23]. However, the current predictive modelling at these extremely low p_0 levels has not been compared with experimental data, as operating current devices at such low p_0 is not feasible. For example, the current Townsend breakdown model in DYON assumes instantaneous breakdown along the open field lines once $\alpha^* L_{open} > 0.5$ is met. This assumption is valid for the modelling of current devices. If the breakdown phase takes significantly longer during low-pressure operations in ITER, calculating the breakdown time could improve predictions of I_p evolution and optimise the B_z waveform. Whether and how significant any physical issues not included in the current Townsend breakdown model would emerge at very low p_0 could be verified using high-fidelity particle-in-cell modelling, such as BREAK [20].

Regarding the low p_0 operation in ITER, [25] [26] reported a risk of runaway electron generation during the plasma initiation phase, but it was not included in the modelling in this paper. Significant runaway electron currents could limit the ohmic heating of the plasma, thereby preventing successful burn-through or further ramp-up of the plasma current [27]. Runaway electron generation is a complex function of n_e, T_e, and the toroidal electric field, and must therefore be assessed using self-consistent modelling [2] [28]. Furthermore, the transport of runaway electrons is highly dependent on magnetic configurations. The transition from open magnetic field configurations to the formation of CFSs should be taken into account for runaway electron transport modelling. For this purpose, runaway electron models would necessitate a full electromagnetic model such as DYON.

7. CONCLUSION

Validation of predictive plasma initiation modelling across five different fusion devices (VEST, MAST-U, EAST, DIII-D, and KSTAR) has been performed for the first time in fusion research. It demonstrates the strong generic prediction capability that full electromagnetic DYON modelling can successfully predict inductive plasma initiation in various devices and discharges.

The DYON simulations successfully reproduced the experimental operation spaces using only hardware design specifications and control room input data—specifically coil currents and measured prefill gas pressure—without any free parameter adjustments for individual discharges. The model correctly predicts Townsend breakdown failure, plasma burn-through failure, and successful plasma initiation across all devices. Device-specific modifications were limited to sputtering models dependent on wall material properties, ferromagnetic corrections when necessary, and pressure calibration coefficients. The experimental database reveals that plasma initiation can occur at prefill pressures substantially below conventional Paschen curve predictions using the averaged connection length. This indicates that Townsend breakdown assessment of individual field lines via full electromagnetic modelling is necessary.

Extrapolation to ITER based on the multi-machine validation predicts a wide feasible prefill gas pressure range of 0.01–1.5 mPa for successful plasma initiation, assuming effective first wall boronization and minimal initial impurities (0.1% oxygen). The lower pressure limit is approximately one order of magnitude lower than in current devices, reflecting ITER's significantly longer connection length. However, the burn-through phase is predicted to extend to approximately one second, substantially longer than the 20–30 ms in current devices, due to the larger vacuum volume. Initial impurity content exceeding 5% would restrict the upper pressure limit, emphasising the importance of wall conditioning.

The DYON code, validated across diverse tokamak configurations, is now established as a reliable predictive tool for assessing inductive plasma initiation feasibility and optimising operating scenarios. The code is ready for application to the design assessment of planned future devices including ITER, EU-DEMO, and STEP, and serves as a platform for integrating additional physics models such as pre-ionisation, non-inductive current drive, and heating assistance with RF waves.

ACKNOWLEDGEMENTS

This work has been carried out within the framework of the EUROfusion Consortium, funded by the European Union via the Euratom Research and Training Programme (Grant Agreement No. 101052200–EUROfusion) and from the EPSRC (Grant Number EP/W006839/1). This work was also supported in part by the U.S. Department of Energy Award DE-AC05-00OR22725. This research has also been supported by the Brain Korea 21 FOUR Program (No. 4199990314119). To obtain further information on the data and models underlying this paper please contact PublicationsManager@ukaea.uk∗. Views and opinions expressed are however those of the author(s) only and do not necessarily reflect those of the European Union or the European Commission. Neither the European Union nor the European Commission can be held responsible for them.

REFERENCES

[1] ITER Physics Basis Expert Group on Disruptions, Plasma Control, and MHD, "Chapter 8: plasma operation and control," *Nuclear Fusion,* vol. 39, p. 2577, 1999.

[2] P. C. de Vries et al, "ITER breakdown and plasma initiaiton revisited," *Nuclear Fusion,* vol. 59, p. 096043, 2019.

[3] G. Federici et al, "European DEMO design strategy and consequences for materials," *Nuclear Fusion,* vol. 57, p. 092002, 2017.

[4] Hendrik Meyer, "Plasma burn - mind the gap," *Philosophical Transactions of The Royal Society A,* vol. 382, p. 20230406, 2024.

[5] R. J. Hawryluk et al, "Effects of low Z impurities during the start up phse of a large tokamak," *Nuclear Fusion,* vol. 16, p. 775, 1976.

[6] B. Lloyd et al, "ECRH-assisted start-up in ITER," *Plasma Physics and Controlled Fusion,* vol. 38, p. 1627, 1996.

[7] Hyun-Tae Kim et al, "Enhancement of plasma burn-through simulation and validation in JET," *Nuclear Fusion,* vol. 52, p. 103016, 2012.

[8] Hyun-Tae Kim et al, "Physics of plasma burn-through and DYON simulations for the JET ITER-like wall," *Plasma Physics and Controlled Fusion,* vol. 53, p. 083024, 2013.

[9] V.A. Belyakov et al, "Plasma initiation stage analysis in tokamaks in TRANSMAK code," *Plasma Devices Operation,* vol. 11, pp. 193-202, 2003.

[10] G. Granucci et al, "Experiments and modeling on FTU tokamak for EC assisted plasma start up stdies in ITER-like configuration," *Nuclear Fusion,* vol. 55, p. 093025, 2015.

[11] Hyun-Tae Kim et al, "Benchmarking of codes for plasma burn-through in tokamaks," *Nuclear Fusion,* vol. 60, p. 126049, 2020.

[12] Hyun-Tae Kim et al, "Development of full electromagnetic plasma burn-through model and validation in MAST," *Nuclear Fusion,* vol. 62, p. 126012, 2022.

[13] Hyun-Tae Kim et al, "Validation of prediction capability of operating space for plasma initiation in MAST-U," *Nuclear Fusion,* vol. 64, p. 126010, 2024.

[14] Hong-Sik Yun et al, "Improvement and validation of plasma initiation model for Versatile Experiment Spherical Torus," in *29th IAEA Fusion Energy Conference,* London, 2023.

[15] Runze Chen et al, "Validation of DYON simulations and development of physical sputtering models for lithiation and boronisation in EAST," *Nuclear Fusion,* vol. 65, p. 076043, 2025.

[16] Y. Gribov et al, "Progress in the ITER Physics Basis Chapter 8: Plasma operation and control," *Nuclear Fusion,* vol. 47, p. S385, 2007.

[17] E. A. Lazarus et al, "Using a multipole expansion for startup in the DIII-D tokamak," *Nuclear Fusion,* vol. 38, p. 1083, 1998.

[18] Jayhyun Kim et al, "Stable plasma start-up in the KSTAR device under various discharge conditions," *Nuclear Fusion,* vol. 51, p. 083034, 2011.

[19] M. Valovic , "Convective losses during current initiation in tokamaks," *Nuclear Fusion,* vol. 27, p. 599, 1987.

[20] Min-Gu Yoo et al, "Evidence of a turbulent ExB mixing avalanche mechanism of gas breakdown in strongly magnetized systems," *Nature Communications,* vol. 9, p. 3523, 2018.

[21] Ximan Li et al, "Development of plasma burn-through simulation code and validation in SUNIST-2 and EAST," *Nuclear Fusion,* vol. 65, p. 066017, 2025.

[22] R. A. Pitts et al, "Plasma-wall interaction impact of the ITER re-baseline," *Nuclear Materials and Energy,* vol. 42, p. 101854, 2025.

[23] Hyun-Tae Kim et al, "Plasma burn-through simulations using the DYON code and predictions for ITER," *Plasma Physics and Controlled Fusion,* vol. 55, p. 124032, 2013.

[24] F. Imbeaux et al, "Design and first applications of the ITER integrated modelling and analysis suite," *Nuclear Fusion,* vol. 55, no. 12, p. 123006, 2015.

[25] Y. Gribov et al, "Progress in simulation of ITER First Plasma operation (P1.1075)," in *45th EPS Plasma Physics Conference*, Prague, Czech, 2018.

[26] Y. Lee et al, "Binary Nature of Collisions Facilitates Runaway Electron Generation in Weakly Ionized Plasmas," *Physical Review Letter*, vol. 133, p. 175102, 2024.

[27] M. Hoppe, "Runaway electron generation during tokamak start-up," *Journal of Plasma Physics*, vol. 88, no. 3, p. 905880317, 2022.

[28] P. C. de Vries et al, "Cross-machine comparison of runaway electron generation during tokamak start-up for extrapolation to ITER," *Nuclear Fusion*, vol. 63, no. 8, p. 086016, 2023.